

# BUILDING RECOGNITION BASED ON AIRBORNE AND SPACE BORNE INSAR DATA

A. Thiele a, \*, H. Hammer a, E. Cadario a, K. Schulz a, U. Soergel b

a FGAN-FOM Research Institute for Optronics and Pattern Recognition, Gutleuthausstrasse 1, 76275 Ettlingen, Germany - (thiele, hammer, cadario, schulz)@fom.fgan.de

b Institute of Photogrammetry and GeoInformation, Leibniz Universität Hannover, Nienburger Strasse 1, 30167 Hannover, Germany - soergel@ipi.uni-hannover.de

Commission VII, WG VII/2

**KEY WORDS: SAR, interferometry, building reconstruction, airborne and space borne data**

## ABSTRACT:

Because of its independence of time of day and its all weather capability, synthetic aperture radar (SAR) has become a key remote sensing technique in the last decades. In the past, spatial resolution of space borne SAR systems was rather coarse, so the exploitation of building signature and even the reconstruction of buildings in dense urban areas based on InSAR data was restricted to commercial and modern experimental airborne SAR systems. These are capable of providing single pass InSAR data with spatial resolution well below half a meter and much better. Now, the new generation of space borne SAR satellites (e.g. TerraSAR-X, RADARSAT-2, or COSMO-SkyMed) allows a more detailed analysis at the object level even for urban areas. This gives rise to the question: Is it possible to transfer basic algorithms of building reconstruction based on airborne sensors to such data? Because of the high availability and short repeat time of the space borne sensors, they are particularly useful e.g. in case of disaster management. In this paper a known algorithm of gable-roofed building reconstruction is applied to airborne and space borne InSAR data of the same test site. The algorithm exploits the appearance of buildings in magnitude images, which is dominated by effects of the inherent oblique scene illumination, such as layover, radar shadow and salient lines of bright scattering caused by direct reflection or multipath signal propagation. Especially, in urban residential districts often salient pairs of parallel lines of bright magnitude are caused by gable-roofed buildings. By exploitation of this magnitude signature, building hypotheses are assembled. The ambiguity in the group of building hypotheses can be solved by considering additional information and by investigation in the interferometric phase signature. Therefore, interferometric phases are simulated based on the intermediate 3D building hypotheses and finally compared with the real interferometric phases. The hypothesis showing higher correlation with the real phases is chosen as final reconstruction result. The quality assessment of the reconstruction results is supported by high-resolution LIDAR data and cadastral data. The study is carried out on airborne AeS-1 and space borne TerraSAR-X data.

## 1. INTRODUCTION

Synthetic Aperture RADAR (SAR) is capable of delivering data at any time and under bad weather conditions, which leads to the fact that SAR become a key remote sensing technique in the last decades. Because of the rather coarse spatial resolution of space borne SAR sensors, the analysis of such data was often restricted to radiometric image properties, which is for example useful for land cover classification. The analysis of settled areas was restricted to commercial airborne SAR systems, capable to provide single pass InSAR data with spatial resolution well below half a meter, and modern experimental sensors, achieving geometric resolution of amplitude data in the decimetre scale. Recently published work concerning building detection and reconstruction in urban areas using high resolution SAR and InSAR data are (Soergel et al., 2003), (Simonetto et al., 1999), and (Xu et al., 2007). It was shown, that by exploitation of the building signature, which is characterized by phenomena such as foreshortening, layover, occlusions, total reflection, and multi-bounce scattering, even the reconstruction of buildings in dense urban areas is possible. Furthermore, in (Xu et al., 2007) and (Thiele et al., 2007a) a significant improvement of the building recognition results could be shown by combining multi-aspect data. The additional investigation in InSAR data,

especially in the phase distribution in the layover area, was presented in (Cellier, 2007) and (Thiele et al., 2008b).

Now the new generation of space borne SAR satellites (e.g. TerraSAR-X, RADARSAT-2, or COSMO-SkyMed), featuring a slant range resolution of up to 1 meter, allows a more detailed analysis at the object level even for urban areas. This gives rise to the question: Is it possible to transfer basic algorithms of building reconstruction based on airborne data to such space borne data? Since space borne data is highly available and the repeat time is short, such data is highly useful e.g. in case of disaster management.

In this paper a known algorithm of gable-roofed building reconstruction (Thiele et al., 2008a) is applied to airborne and space borne InSAR data at the same test site. In Section 2 the sensor and scene data and especially the interferogram calculation are described. The appearance of gable-roofed buildings in InSAR data is discussed in Section 3. The steps of building recognition and reconstruction are described in Section 4. Furthermore, in Section 5 the results are presented and the potentials are discussed.

## 2. AIRBORNE AND SPACE BORNE SAR SENSORS

Building recognition and reconstruction in the past was limited to airborne SAR systems, due to the achieved resolution. The

---

\* Corresponding author. This is useful to know for communication with the appropriate person in cases with more than one author.

	<b>AeS-1</b>	<b>TerraSAR-X</b>
<b>Sensor Parameters</b>		
Company	INTERMAP Technologies	DLR, Infoterra
Wavelength	0.0314 m [X-Band]	0.0311 m [X-Band]
Range and azimuth pixel spacing	0.3747 m, 0.1518 m	0.4547 m, 0.8700 m
Polarization	HH	HH
<b>Scene Parameter</b>		
Acquiring Date	2003-03-13	2008-07-22, 2008-08-02
Scene Size	2,300 m x 5,600 m	7,000 m x 5,000 m
First range bin distance	3,530 m	664,541 m
Off-nadir angle Near, middle, far range	28°, 40°, 52°	40.9°, 41.2°, 41.5°
Sensor altitude	3,191.4 m	503,442 m
Baseline	2.4 m	30.4 m

Table 1. Summary of sensor and scene parameters of airborne sensor AeS-1 and space borne sensor TerraSAR-X

new generation of space borne SAR systems provides image resolutions comparable of former airborne systems. In the following, two sensor systems are characterized and the necessary pre-processing of the data is described.

## 2.1 System Parameters

The study is carried out using airborne AeS-1 (Schwaebisch et al., 1999) and space borne TerraSAR-X data. The AeS-1 sensor was a commercial SAR system of INTRMAP Technologies, which provided data with a resolution below half a metre. The most important sensor and scene parameters are listed in Table 1. Nowadays, other commercial airborne systems such as STAR3i (Bullock et al., 1997) provide similar resolutions. Additionally, with experimental SAR systems such as PAMIR (Brenner et al., 2008) even resolutions in the decimetre scale are possible.

The TerraSAR-X sensor is the first commercial SAR satellite which achieves resolutions up to 1 meter in the high-resolution spotlight mode. The most important parameters of this product relating to our scene and study are listed in Table 1.

## 2.2 Preparation of InSAR Data

In this section the necessary pre-processing of the interferometric image pairs is described by considering own and commercial software components.

### 2.2.1 Single-Pass Airborne InSAR Data (e.g. AeS-1)

The AeS-1 sensor recorded data in single-pass PingPong mode. The image pair is given as single look complex data in slant range geometry. Due to the baseline established by the geometric separation of the antennas, the two SAR images show different range/azimuth coordinate grids. Therefore, a co-registration is required. Since SAR interferometry relies on the phase difference of two complex SAR images, sub-pixel accuracy is a prerequisite. This sub-pixel registration is realized by image oversampling and coherence maximization. The subsequent interferogram generation includes multi-look filtering, followed by flat earth correction, phase centering and

phase correction. By the step of phase centering a phase distribution with zero mean is achieved. This is necessary to make the comparison of real and simulated phase profiles possible (Thiele et al., 2007b). For some cases subsequent phase correction is useful to reduce phase ambiguities at building locations (Thiele et al., 2007a).

### 2.2.2 Repeat-Pass Space Borne InSAR Data (e.g. TerraSAR-X)

The interferometric image pair of high-resolution spotlight TerraSAR-X data is given as single look complex data in slant range geometry. The data were acquired in repeat-pass mode with eleven days' time lack. The necessary co-registration of the image pair is realized by using the commercial software tool ENVI. Subsequently, the step of flat earth correction is also passed by the use of this software. Since multi-look filtering in ENVI is attended by a reduction of the image size, this step is not carried out with this software. Furthermore, just as for the airborne data, the phase centring and phase correction are performed by using own software tools.

## 3. APPEARANCE OF GABLE-ROOFED BUILDINGS

In the following the known appearance of gable-roofed buildings in magnitude and phase data is shortly described by showing real signatures of airborne and space borne InSAR sensors. The focus is on the characterization of the differences between both recording systems.

### 3.1 Magnitude Data

Due to the side looking viewing geometry of SAR sensors, the magnitude signature of a building is characterized by a layover area, a corner reflector between ground and building wall, a roof signal, and a radar shadow region. Those are shown in Figure 1a for a gable-roofed building.

The first building signal (i.e. smallest distance to the sensor) is the so-called layover area, which usually appears bright due to a superposition of backscatter from ground, façade, and roof. A subdivision of the layover area is given in some cases according to building dimensions and illumination geometry. This effect

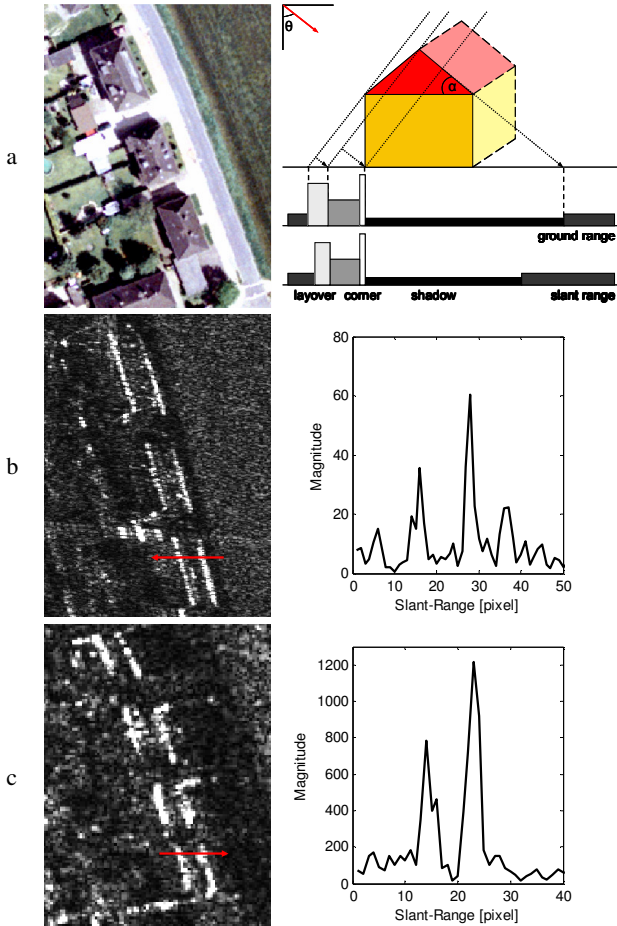


Figure 1. A group of hip-roofed buildings in optical image and schematic view of magnitude appearance of gable-roofed building (a), AeS-1 data of same group and corresponding magnitude profile marked in red (b), TerraSAR-X image and magnitude profile (c)

occurs frequently at gable-roofed buildings such as shown here, due to their pitched roof area. The maximum amplitude and width of the layover peak depends on interrelation between roof pitch, off-nadir angle, and span angle.

The adjacent low intensity part results from direct reflection of ground and wall. The second peak is caused by the dihedral corner spanned by ground and building wall. Both maxima appear as long lines along the entire side of the building (Figure 1b,c). A single backscattering from the building roof is not observable for this kind of building and viewing geometry. A dark region caused by the building shadow is visible behind the double peak signature. The described appearance is also observable in the given magnitude profiles of airborne and space borne data, in spite of the opposite viewing directions.

### 3.2 Phase Data

Beside the significant magnitude signature, also the phase signature comprises interesting features, which are necessary for the subsequent building reconstruction.

The phases are also characterized by the SAR effects layover, multi-bounce reflection, and shadow, due to gable-roofed buildings. In Figure 2a the LIDAR signature of the hip-roofed building group and a corresponding height profile are given. The corresponding interferometric phases of the airborne

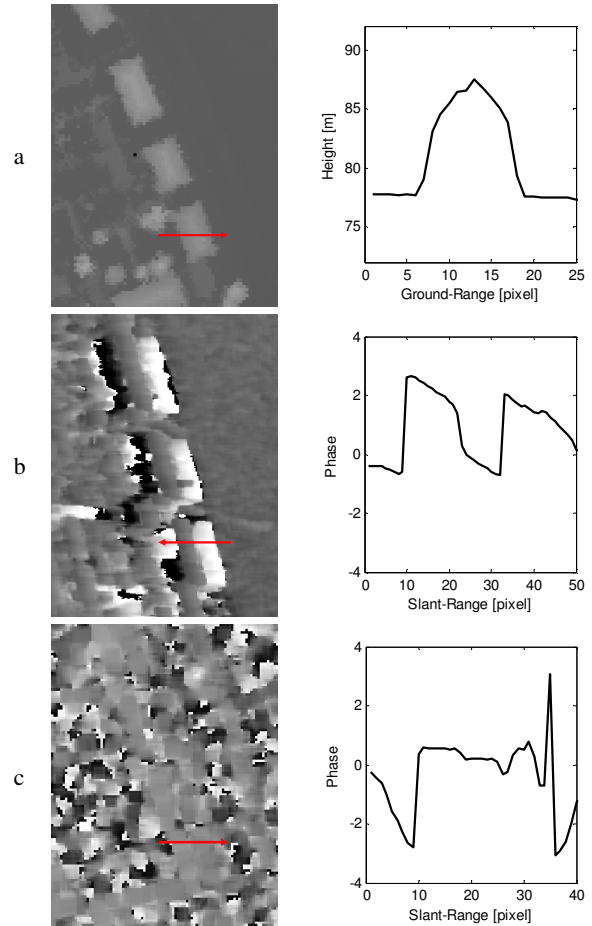


Figure 2. LIDAR DSM of building group and corresponding height profile (a), AeS-1 interferometric phase image and profile of one building (b), TerraSAR-X interferometric phases and profile (c)

system AeS-1 (b) and the space borne system TerraSAR-X (c) are depicted as well.

In detail, just as the magnitude value, the interferometric phase of a single range cell results from a mixture of the backscattering signal of different contributors. Hence, the resulting interferometric phase of an image pixel is a function of heights from all contributors. Therefore, the layover area of a building is affected by heights of terrain, building wall and its roof. Consequently, the shape of the phase profiles is among others dominated by building geometry.

As observable in Figure 2b, the resulting phase in the layover area is dominated by the backscattering of the building roof. This was also the case in the magnitude profile, resulting in a bright line. Consequently, the phase value at the beginning of the layover area is much higher than the phases of the rest of the layover area. The downward shape of the layover phases results from the mixture of information from the two backscatterers ground and building wall, where the height of the building wall shows a constant downward trend. Behind the layover area, the corner point shows a low interferometric phase value approximately at terrain level. This analysis shows that the geometric information of buildings is mainly contained in the layover area, which gives rise to considering the interferometric phases in the building reconstruction process.

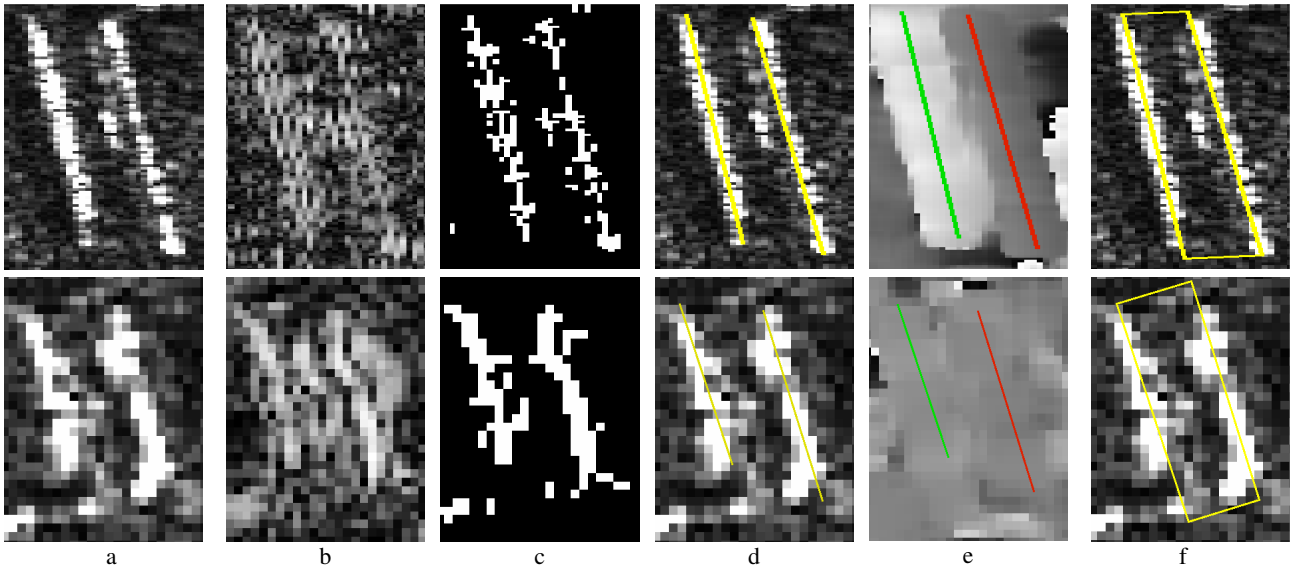


Figure 3. Overview of the processing steps of feature segmentation in AeS-1 data (first row) and TerraSAR-X data (second row); magnitude input image (a), one probability image (b), post-processed hint image (c), result of line detection (d), result of line filtering based on interferometric phases (e), result of parallel line assembly (f)

#### 4. RECOGNITION AND RECONSTRUCTION

In the following section the building recognition and reconstruction based on the exploitation of magnitude data and interferometric phase data is described and shown for one building recorded by AeS-1 and TerraSAR-X.

##### 4.1 Segmentation of Building Features

The segmentation of the building primitives starts with the exploitation of the significant magnitude signature observable for parallel configurations of ridge orientation and azimuth direction. The perviously described ‘double lines’ are segmented using a SAR specific operator developed by Tupin (Tupin et al., 1998), which works on the original magnitude images. This template detector determines the probability of a pixel of belonging to a line.

The results presented here are achieved by considering eight different template orientations based on a central window and two neighbouring windows of the same size. One of the eight probability images is shown in Figure 3b. The subsequent line segmentation considers a magnitude and a probability threshold. The magnitude threshold enables to differentiate between light and dark lines. This threshold had to be chosen individually for the AeS-1 and TerraSAR-X data. A resulting ‘hint image’ (ones for every orientation) is given in Figure 3c. Based on these images straight lines are fitted, where only those are considered as correct that show the same orientation as the respective template orientation. In a subsequent prolongation step small segments are merged to longer lines by considering gap distance and orientation of segments. Results of the line detection are given in Figure 3d.

The next step comprises the assembly and filtering of ‘double line’ constellations. Finally, a gable-roofed hint should be found. Hence, parallel lines are assembled by matching a distance threshold and a maximum orientation difference. Furthermore, the sensor close line has to show a higher mean phase value than the second line (‘corner line’), due to the described phase signature of buildings in the layover area. In Figure 3e the higher ‘layover line’ is marked in green and the lower ‘corner line’ in red. If this phase distribution is not

fulfilled the assembled ‘double line’ is not considered further as a building hint. A final segmentation result is given in Figure 3f.

##### 4.2 Extraction of Building Parameters

In the next step, based on the segmented ‘double line’ constellation, building parameters are assembled, which enable the formulation of building hypotheses. In the slant range geometry the building parameters  $a$  and  $b$  are extracted. Parameter  $a$  is characterized by the distance between the two maxima, and is equal to the ‘double line’ width. The second one, parameter  $b$ , is defined as width of the layover maximum.

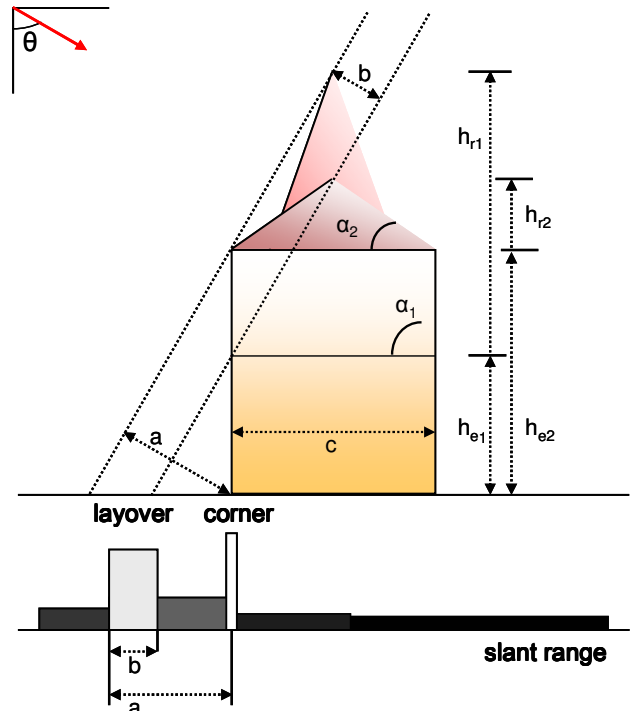


Figure 4. Schematic presentation of the two remaining building hypotheses  $\alpha > \theta$  (index 1) and  $\alpha < \theta$  (index 2)

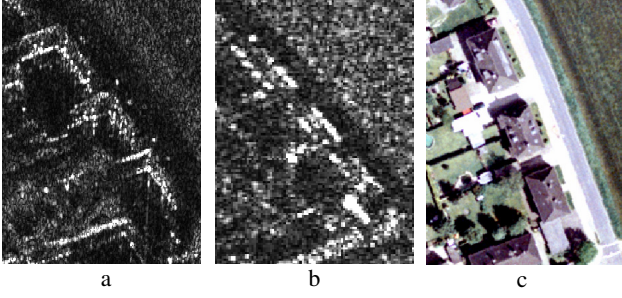


Figure 5. Summary of multi-aspect information; orthogonal view AeS-1 (a), descending orbit TerraSAR-X (b), optical image (c)

This can be extracted during the line detection step or an additional edge detection step (Thiele et al., 2008a). Based on these two parameters two groups of building hypotheses can be assembled, which show the same magnitude signature. One example of every group is depicted in Figure 4. The first model, indicated by 1, shows a roof pitch angle  $\alpha_1$  greater than the off-nadir angle  $\theta$ , the second model a pitch angle  $\alpha_2$  smaller than the off-nadir angle  $\theta$ .

The resulting ambiguity problem can be reduced to two building hypotheses by the extraction of the building width, here defined by the parameter  $c$  (Figure 4).

This was successfully shown by exploiting an orthogonal viewing direction of AeS-1 data (Thiele et al., 2007a). Furthermore, the use of the contrary orbit of space borne data as well as the investigation in optical images (Wegner et al., 2009) has to be tested in the future. Such kind of possible data are given in Figure 5 showing the same test site.

Based on these three parameters, two 3D building hypotheses can be formulated. In Figure 4,  $h_e$  defines the height from ground up to eaves and  $h_r$  the height up to ridge. In (1) and (2)  $h_e$ ,  $h_r$ , and  $\alpha$  are given for the two cases.

$$\alpha_1 > \theta, \quad h_{e1} = \frac{(a-b)}{\cos \theta}, \quad h_{r1} = h_{e1} + \frac{c}{2} \cdot \tan \alpha_1 \quad (1)$$

$$\tan \alpha_1 = \tan \theta + 2 \frac{b}{c \cdot \cos \theta}$$

$$\alpha_2 < \theta, \quad h_{e2} = \frac{a}{\cos \theta}, \quad h_{r2} = h_{e2} + \frac{c}{2} \cdot \tan \alpha_2 \quad (2)$$

$$\tan \alpha_2 = \tan \theta - 2 \frac{b}{c \cdot \cos \theta}$$

The decision between the resulting two building hypotheses can be carried out by the use of the simulation of interferometric phases, which is described and carried out in the next section.

#### 4.3 Assessment of Building Hypothesis

In the reconstruction approach, the single analysis of the magnitude signature leads to an ambiguity problem. The resulting two building hypotheses were shown in Figure 4. By focusing now on the analysis of the interferometric phases the problem can be solved. Therefore, based on the given building hypotheses interferometric phases are simulated by using the algorithm presented in (Thiele et al., 2007b). It takes into account that especially at building locations the interferometric phase of a single range cell is a mixture of several contributions. Hence the most interesting signature part is the layover region.

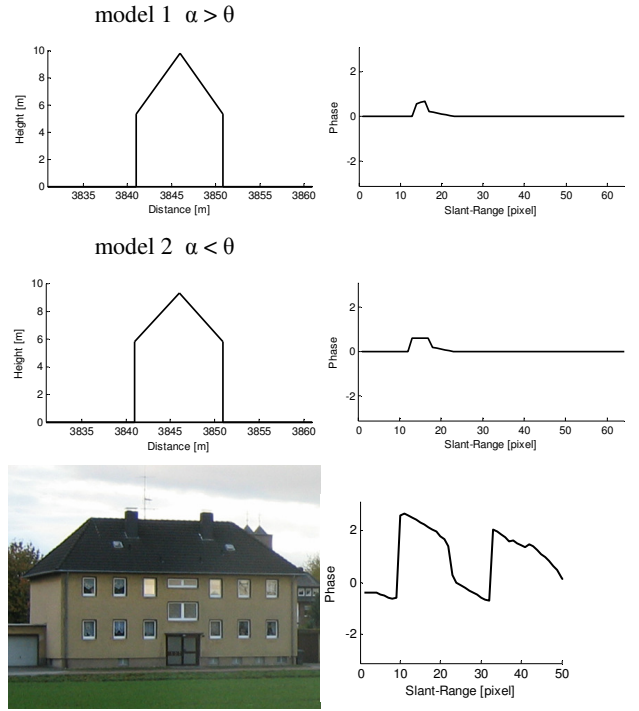


Figure 6. DSM profile and simulated InSAR phase profiles based on reconstruction hypotheses  $\alpha > \theta$  and  $\alpha < \theta$ , optical image of real building and real InSAR phase profile

The two resulting phase profiles (Figure 6) show that different groups of contributors are forming a different layover phase shape.

Caused by the different  $h_r$  of the building hypotheses the first phase value in the layover area is different. Furthermore, the phase distributions show different descents, due to the mixture of heights of the different contributors. The first layover part of hypothesis  $\alpha > \theta$  is characterized by the contributors roof and ground. In contrast, the same part of hypothesis  $\alpha < \theta$  is characterized by backscatter of roof, wall and ground. Consequently, the descent is weaker. The subsequent part of the layover shows a similar shape for both hypotheses, due to the fact that the two contributors – wall and ground – show the same height.

For a real assessment of the two hypotheses the similarity between the simulated and real phases is determined by calculating the differences and the correlation coefficient. First assessment results were presented in (Thiele et al., 2008a), but at this stage it was not part of the study.

## 5. RESULT AND CONCLUSION

The building recognition and reconstruction based on airborne and space borne data by using the same approach was goal of this study. The final results of both datasets by focusing on one building are listed in Table 2. Furthermore, the ground truth data extracted by cadastral and LIDAR DSM data are given as well.

First, the extraction of the building width was not part of this test, which explains the constant value for all building width data. The most important result was, that the building recognition and furthermore the reconstruction based on the space borne data was successful.

building parameter	$\theta$ [°]	length [m]	width [m]	$\alpha$ [°]	$h_c$ [m]	$h_r$ [m]
<b>AeS-1</b>						
model 1 $\alpha > \theta$	39	15.9	9	42	5.3	9.8
model 2 $\alpha < \theta$	39	15.9	9	35	5.8	9.3
<b>TerraSAR-X</b>						
model 1 $\alpha > \theta$	41	19.5	9	45	4.8	9.4
model 2 $\alpha < \theta$	41	19.5	9	36	5.4	8.8
<b>ground truth</b>		16	9	42	6	10

Table 2. Results of the building reconstruction

Focusing on the reconstruction results, the length of the building was more accurately detected in the AeS-1 data. This was caused by an extracted corner line that was too long. In comparison, considering the parallel extracted layover line for the assembly of the hypothesis the building length would be 16.6 m.

The reconstruction of the building height achieved good results as well as the pitch angle extraction. For these three parameters the absolute differences to the ground truth data are less reliable, because the extraction from the one meter spacing LIDAR DSM could be inexact.

Future studies will be focused on the exploitation of additional datasets for the extraction of the building width. Furthermore, the accuracy and robustness of the extraction of parameters  $a$  and  $b$  will be investigated, using different filtering windows used for SAR processing.

## 6. ACKNOWLEDGMENT

We want to thank Infoterra GmbH for providing the TerraSAR-X data.

## 7. REFERENCES

Brenner, A.R., Roessing, L. 2008. Radar Imaging of Urban Areas by Means of Very High-Resolution SAR and Interferometric SAR. *IEEE Transactions on Geoscience and Remote Sensing*, Vol. 46, No. 10, pp. 2971-2982.

Bullock, M.E., Lawrence, G., Darns, R.V., and Tennant, K. 1997. Map generation utilizing IFSARE imagery and digital elevationsmodels from the Intermap STAR-3i system. *Proceedings of IGARSS*, Vol. 3, pp. 1350-1357.

Cellier, F. 2007. "Reconstruction 3D de bâtiments en interférométrie RSO haute résolution approche par gestion d'hypothèses", Ecole nationale supérieure des télécommunications: Ph. D. Thesis.

Schwaebisch, M., Moreira, J. 1999. The high resolution airborne interferometric SAR AeS-1. In: *Proceedings of the Fourth International Airborne Remote Sensing Conference and Exhibition*, Ottawa, Canada, pp. 540-547.

Simonetto, E., Oriot, H., Garello, R. 2005. Rectangular building extraction from stereoscopic airborne radar images. *IEEE Transactions on Geoscience and Remote Sensing*, Vol. 43, No. 10, pp. 2386-2395.

Soergel, U., Thoennessen, U., Stilla, U. 2003. Iterative Building Reconstruction in Multi-Aspect InSAR Data. In: Maas

HG, Vosselman G, Streilein A (eds) 3-D Reconstruction from Air-borne Laserscanner and InSAR Data, *IntArchPhRS*, Vol. 34, Part 3/W13, pp. 186-192.

Thiele, A., Cadario, E., Schulz, K., Thoennessen, U., Soergel, U. 2007a. Building recognition from multi-aspect high resolution InSAR data in urban area. *IEEE Transactions on Geoscience and Remote Sensing*, Vol. 45, No. 11, pp. 3583-3593.

Thiele, A., Cadario, E., Schulz, K., Thoennessen, U., Soergel, U. 2007b. InSAR Phase Profiles at Building Locations. *Proceeding of ISPRS Photogrammetric Image Analysis*, Vol. XXXVI, Part 3/W49A, pp. 203-208.

Thiele, A., Cadario, E., Schulz, K., Thoennessen, U., Soergel, U. 2008a. "Reconstruction of residential buildings from multi-aspect InSAR data", *Proceedings of ESA-EUSC Workshop, Frascati, Italy*, available [http://earth.esa.int/rtd/Events/ESA-EUSC\\_2008/](http://earth.esa.int/rtd/Events/ESA-EUSC_2008/), 6p.

Thiele, A., Cadario, E., Schulz, K., Thoennessen, U., Soergel, U. 2008b. Reconstruction of residential buildings by detail analysis of multi-aspect InSAR data. *Proceedings of SPIE, Remote Sensing for Environmental Monitoring, GIS Applications, and Geology VIII*, Cardiff, Wales, Vol. 7110, pp. 71100H-1-8.

Tupin, F., Maitre, H., Mangin, J.-F., Nicolas, J.-M., Pechersky, E. 1998. Detection of Linear Features in SAR Images: Application to Road Network Extraction. *IEEE Transactions on Geoscience and Remote Sensing*, Vol. 36, No. 2, pp. 434-453.

Wegner, J.D., Soergel, U., Thiele, A. 2009. Building extraction in urban scenes from high-resolution InSAR data and optical imagery. To be published in *Proceedings of Urban Remote Sensing Joint Event*, Shanghai, China.

Xu, F., Jin, Y.-Q., 2007. Automatic Reconstruction of Building Objects From Multiaspect Me-ter-Resolution SAR Images. *IEEE Transactions on Geoscience and Remote Sensing*, Vol. 45, No.7, pp. 2336-2353.